Opto-Electronics Review 30 (2022) e140551

PAN POLISH ACADEMY OF SCIENCES

Opto-Electronics Review

journal homepage: https://journals.pan.pl/opelre

Van der Waals materials for HOT infrared detectors: A review

Antoni Rogalski

Institute of Applied Physics, Military University of Technology, 2 Kaliskiego St., 00-908 Warsaw, Poland

Article info

Article history:
Received 22 Jan. 2022
Received in revised form 4 Feb. 2022
Accepted 13 Feb. 2022
Available on-line 11 Mar. 2022

Keywords:
2D material photodetectors; transition metal dichalcogenides photodetectors; HgCdTe photodiodes; high operating temperature infrared detectors.

Abstract

In the last decade several papers have announced usefulness of two-dimensional materials for high operating temperature photodetectors covering long wavelength infrared spectral region. Transition metal dichalcogenide photodetectors, such as $PdSe_2/MoS_2$ and WS_2/HfS_2 heterojunctions, have been shown to achieve record detectivities at room temperature (higher than HgCdTe photodiodes). Under these circumstances, it is reasonable to consider the advantages and disadvantages of two-dimensional materials for infrared detection. This review attempts to answer the question thus posed.

1. Introduction

Discovery of graphene in 2004 and later on many other two-dimensional (2D) materials caused their intensive researches in world-wide laboratories. Their extraordinary and unusual electronic and optical properties also indicate a promising application in infrared (IR) detector technology. Up till now, however, the place of 2D materials in a wide infrared detector family is not assessed. According to the author's knowledge, this topic is generally omitted in the literature. The partial answer to this question is given in the recently published monograph [1].

The present paper tries to predict future position of 2D materials as high operating temperature (HOT) sensors in a long wavelength infrared (LWIR) spectral range. Some conclusions result from the history of infrared detectors, other conclusions—from the present status and trends in their development.

HgCdTe ternary alloy takes dominant position in IR detector technology, particularly in the LWIR region (8 to 12 μm). This material system also inspired the development of four generations of IR systems [2]. In the paper published in 2003 [3] on HgCdTe position, it was written: *Over the last 40 years it has successfully fought off major challenges from extrinsic silicon and lead-tin telluride devices. Despite that, however, it has more competitors today than ever before. These include Schottky barriers on silicon, SiGe heterojunctions, AlGaAs multiple quantum wells, GaInSb strain layer superlattices, high-temperature superconductors, and especially two types of thermal detectors: pyroelectric detectors and silicon bolometers. It is interesting, however, that none of these is competitive in terms of fundamental properties. They may promise to be more easily manufactured, but never to provide higher performance or, with the exception of thermal detectors, to operate at higher or even comparable temperatures*. In the last decade, a new class of materials emerged as a competitor to HgCdTe; 2D materials. The question is: will the discovery of 2D materials affect the HgCdTe status? The present paper, almost 20 years later, attempts to answer this question.

First, different requirements (figure of merit) are specified for single-element detectors and focal plane arrays implemented in the IR system. The requirements are different, as clearly highlighted in section 2. They have been discussed in detail in several recently published papers [4–6] and are repeated briefly below. Section 3 compares the basic physical properties of HgCdTe and 2D materials used for detectors in the LWIR range. The influence of two important material parameters, absorption coefficient and carrier lifetime, on the performance of IR detectors is considered in section 4. Section 5 deals with the current state-of-the-art of HOT IR photodetectors, including "Law 19" as a new reference benchmark. Since the focal plane array (FPA) commercialization process does not depend only on the detector performance, but on a

*Corresponding author at: antoni.rogalski@wat.edu.pl

https://doi.org/10.24425/opelre.2022.140551
1896-3757/ Association of Polish Electrical Engineers (SEP) and Polish Academic of Sciences (PAS). Published by PAS

fabrication of large-scale high-quality detector materials at a low cost, these aspects are discussed in the final sections.

2. Figure of merit for single infrared detectors and arrays

Different figures of merit are used to determine the quality of single-element IR photodetectors and arrays.

2.1. Single-element photodetectors

As is shown by Piotrowski and Rogalski [7], the performance of IR photodetectors is limited by the statistical nature of generation and recombination mechanisms in the semiconductor. Thermal processes in the device material limit the detectivity of the optimized IR photodetector. It can be expressed by:

$$D^* = k\frac{\lambda}{hc}\left(\frac{\alpha}{G_{th}}\right)^{1/2}. \tag{1}$$

λ is the wavelength, h is the Planck's constant, c is the speed of light, α is the absorption coefficient, and G_{th} (in $cm^{-3}s^{-1}$) is the thermal generation in the active detector region, k is the coefficient dependent on radiation coupling of a detector including, e.g., antireflection coating, microcavities, or plasmonic structures. α/G_{th} is the ratio of the absorption coefficient to the thermal generation rate. As can be seen, this ratio is the figure of merit of any infrared detector material. This figure of merit can be utilized to predict the ultimate performance of any infrared detector and select materials that can be used as detector active region.

The ultimate goal of the IR detector technology is the fabrication of photodetectors operating under background limited conditions at possible high temperature when the detector dark current is smaller than the background flux current and $1/f$ noise is negligibly small in comparison to the shot noise of the background flux [4, 8].

The sum of the optical (G_{op}) and thermal generation (G_{th}) rates defines the total generation rate:

$$G = G_{th} + G_{op}. \tag{2}$$

The cryogenic cooling is usually used to suppress thermal generation to the lowest possible level and, in this way, to achieve a high signal-to-noise (S/N) ratio (high performance). For practical reasons, it is required to reduce the thermal generation below the optical generation.

Optical generation is due to the signal and background radiation. In the longer wavelength IR range, the background radiation is typically higher compared to the signal radiation. If the influence of the background flux level is stronger than the thermal generation, the performance of the device is determined by the background radiation [the ideal working mode for the infrared detector is to work in background limited infrared photodetector (BLIP) conditions]. Such condition may be described as:

$$\frac{\eta\Phi_B\tau}{t} > n_{th}. \tag{3}$$

where n_{th} is the density of thermal carriers, τ is the carrier lifetime, and Φ_B is the total background photon fluxes density (unit: $cm^{-2}s^{-1}$) reaching the detector, and t is the thickness of the detector. By re-arranging (3), the BLIP requirements are obtained as:

$$G_{op} = \frac{\eta\Phi_B}{t} > \frac{n_{th}}{t} = G_{th}, \tag{4}$$

i.e., the photon generation rate needs to be greater than the thermal generation rate. Both majority and minority carriers can be considered.

2.2. Focal plane arrays

The papers [4, 9] have shown that the detector size (d) and the optics F-number ($f/\#$) are primary parameters of IR systems containing FPA and optics. Since they depend on $F\lambda/d$ (where λ is the wavelength), they affect the detection/identification range, as well as the noise equivalent difference temperature (*NEDT*).

NEDT is a fundamental figure of merit for IR FPAs and characterizes the thermal sensitivity of the IR system. It can be defined as the temperature difference required to produce a unity of the S/N ratio. A smaller *NEDT* value indicates a better thermal sensitivity. Currently, infrared system users prefer a degree of oversampling beyond the diffraction limit, using subwavelength-scale optics enabled by modern nanofabrication (the diffraction-limited pixel size is still relatively large compared to the feature size that can be achieved using state-of-the-art nanofabrication methods) [4, 5]. For an IR system with $f/1$ optics, the smallest practicable detector size should be 2 μm for the mid-wavelength IR (MWIR, 3–5 μm) and 5 μm for the LWIR range [10]. For more realistic $f/1.2$ optics, the smallest practicable detector size is 3 μm and 6 μm for the MWIR and LWIR range, respectively.

On the other side, knowing the detector dark current density, J_{dark}, the background flux (system optics), Φ_B, and the integration time of readout circuit, τ_{int}, *NEDT* can be determined according to relations [8]:

$$NEDT = \frac{1 + (J_{dark}/J_\Phi)}{\sqrt{N_w}\left(\frac{1}{\Phi_B}\frac{d\Phi_B}{dT}\right)}, \tag{5}$$

$$J_\Phi = q\eta\Phi_B, \tag{6}$$

$$N_w = \frac{(J_{dark} + J_\Phi)\tau_{int}}{q}, \tag{7}$$

where N_w is the well capacity of readout, J_Φ is the background flux current, q is the electron charge, A is the detector area, and η is the quantum efficiency. Optics transmission and cold shield efficiency are assumed to be one.

Assuming that $(d\Phi_B/dT)/\Phi_B = C$ is the scene contrast, (5) takes the form of:

$$NEDT = \frac{1 + (J_{dark}/J_\Phi)}{\sqrt{N_w}C} \tag{8}$$

The scene contrast is about 2%/K in the LWIR band.

From the last equation, it follows that if the I_{dark}/J_{ϕ} ratio increases and/or the η value decreases, a longer integration time and a faster optical system are required. This means that faster optics and slower frame rate systems should be used for inefficient detectors. Furthermore, the charge handling capacity of the readout system (N_w), the integration time (τ_{int}), and the dark current of active region (J_{dark}) become the paramount issues for IR FPAs. For example, the very short integration time (for HgCdTe in LWIR typically 200–300 μs) is very useful to freeze a scene with rapidly moving objects. Less effective photodetectors, such as QWIPs, require 10–100 times longer integration times (typically between 5 and 20 ms). QWIP arrays are useful for thermal imaging (where integration time is not critical) but are useless for a target surveillance in guided missiles.

In the above considerations, it was assumed that the temporal detector noise is the main source of noise. However, this stipulation is not true for FPAs where an important source of noise is the nonuniformity (u) in the pixel responses. This nonuniformity is the source of the fixed pattern noise (spatial noise). Figure 1 shows the dependence of the total *NEDT* on the detectivity for different residual nonuniformities (u), assuming a scene temperature of 300 K, and a set of parameters inserted in the figure. Nonuniformity has stronger influence on *NEDT* value than detectivity. It is shown that when the detectivity approaches a value above 10^{10} cmHz$^{1/2}$/W (which is easily achievable at the current stage of detector technology), FPA performance is limited by nonuniformity without correction, and thus, essentially independent of detectivity. Improving the nonuniformity from 0.1% to 0.01% after correction can reduce the *NEDT* from 63 to 6.3 mK.

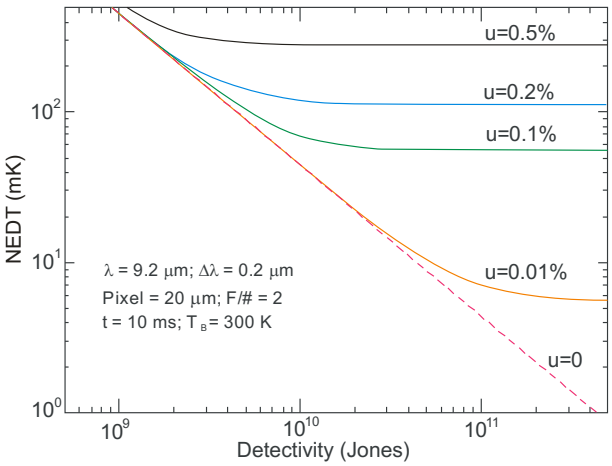

Fig. 1. *NEDT* as a function of detectivity for different levels of nonuniformity u = 0.01%, 0.1%, 0.2%, and 0.5%. Note that for $D^* > 10^{10}$ cmHz$^{1/2}$/W, detectivity is not the relevant figure of merit (after Ref. 2).

The uniformity among pixels within an array is important for accurate temperature measurements, background subtraction, and threshold testing. Nonuniformity value is usually calculated with the standard deviation over the mean, by counting the number of operable pixels in the array. To obtain a low inter-pixel variability and a low *NEDT* value, e.g., below 20 mK, the nonuniformity in response must be less than 0.04%. Such a low value of nonuniformity is not possible in the uncorrected FPA response. To improve the array uniformity, a two-point correction is usually applied [2]. However, improving the FPA uniformity affects the complexity of the IR system by developing compensation algorithms for image correction. In addition, the consumption of a certain number of analogue-to-digital bits reduces the dynamic range of the system.

Due to the strong dependence of the cut off wavelength on the composition x for LWIR $Hg_{1-x}Cd_xTe$ FPAs, the control of material composition is much more stringent for LWIR than for MWIR spectral region.

To summarise the above discussion, it is important to emphasise a clear difference in the figure of merit of single detectors and FPAs. For a single detector, detectivity is an important parameter. In the case of arrays, one of the fundamental parameters is the *NEDT*. The second parameter is the modulation transfer function (*MTF*) [11] which is not considered here.

For thermal imaging systems, the primary performance metrics are thermal sensitivity and spatial resolution. *NEDT* refers to the minimum temperature difference that can be seen above the noise level. *MTF* answers the question: how can a small object image the system? The *MTF* of a system depends on several components and is dominated by the *MTF* of optics, detector, and display and can be cascaded by simply multiplying the *MTF*s components $MTF = MTF_{Optics} \times MTF_{Detector} \times MTF_{Display}$. The *MTF* of an imaging system is limited by the size of the detector and the optic aperture in the spatial frequency range.

3. Fundamental material properties

3.1. HgCdTe

The HgCdTe ternary alloy is an almost ideal material for an infrared detector. Its unique position depends on three key characteristics:

- composition-dependent tailorable energy band gap in the 1–30- μm band,
- high optical coefficients that enable high quantum efficiency, and
- favourable inherent recombination mechanisms that lead to long carrier lifetimes and high operating temperatures.

These unique physical properties of HgCdTe result from the energy band structure of this zinc-blende semiconductor. Furthermore, the HgCdTe alloy system is characterized by both low and high carrier concentration, high mobility of electrons (about 10^4 cm^2/Vs at room temperature for an energy gap below 0.25 eV, see Fig. 2), and low dielectric constant. The very small variation of the lattice constant depending on the composition allows producing high quality heteroepitaxial photodiode structures with performance close to the ultimate limits.

The x-dependence of the mobility is primarily due to the x-dependence of the band gap, and the temperature dependence is due to the competition between different scattering mechanisms that are temperature-dependent. Extremely high mobility values, above 4×10^4 cm^2/Vs, for high-purity samples are observed near the semiconductor-semimetal transition where the electron effective mass has

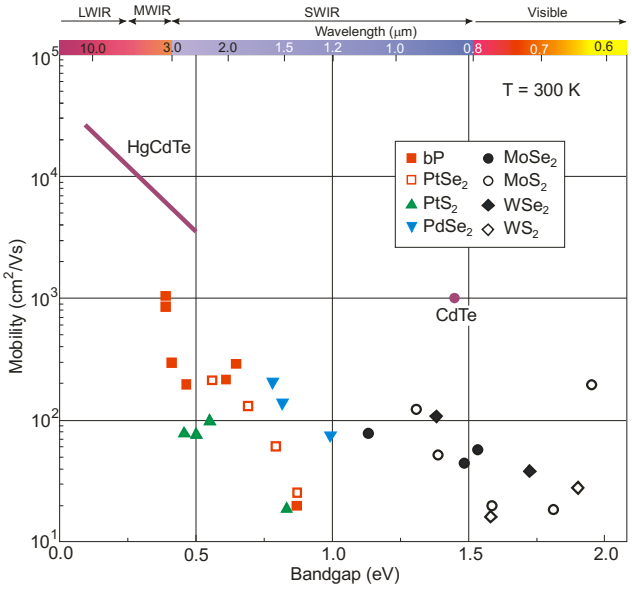

Fig. 2. Electron mobilities in HgCdTe alloy system (after Ref. 12) and layer-dependent room temperature mobilities of group-6 TMDCs, bP, and typical noble TMDs on a back-gated SiO_2 substrate (after Ref. 1).

a minimum value. Higgins *et al.* [12] give an empirical formula for the variation of μ_e with x at 300 K for the very high-quality samples they studied as:

$$\mu_e = 10^4(8.754x - 1.044)^{-1} \quad \text{in cm}^2/\text{Vs}. \tag{9}$$

Table 1 gathers the fundamental material properties of $Hg_{1-x}Cd_xTe$ in comparison with other narrow gap semiconductors used in IR detector technology. The electron m_e^* and the light hole m_{lh}^* effective masses in the narrow-gap HgCdTe are close and can be approximated by $m_e^*/m_0 \approx 0.0071E_g$, where E_g is in eV and m_0 is the free electron mass. The value of the heavy hole $m_{hh}^* = 0.55m_0$ is frequently used in modelling of HgCdTe detectors.

Figure 3 presents the measured intrinsic absorption coefficients for narrow-gap semiconductors used in IR detector technology. The value of the absorption edge in the LWIR range is about 10^3 cm^{-1}; in the MWIR spectral

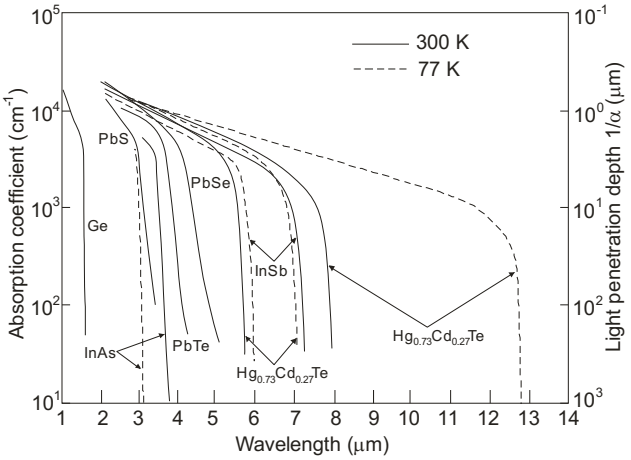

Fig. 3. Spectral dependence of the absorption coefficients for IR photodetector materials.

region it is slightly higher, between 2×10^3 cm^{-1} and 3×10^3 cm^{-1}.

The huge variation of the absorption coefficient near the band gaps of semiconductors, typically about three orders of magnitude, affects the appreciable photocurrent generated by a given semiconductor. The absorption efficiency drops dramatically in the region of the material maximum useful wavelengths. In the region longer than the cut off wavelength, absorption is negligible due to small values of α.

Additional information on the absorption coefficient at room temperature can be found in Fig. 4. The black dots marked for HgCdTe ternary alloys are consistent with the empirical formula for the intrinsic absorption region according to the paper of Chu *et al.* [13]. For other materials, a parabolic band structure is assumed, and the threshold absorption coefficient is estimated for an energy of $1.2E_g$.

As is mentioned above, the favourable inherent recombination mechanisms in HgCdTe lead to long carrier lifetimes and high operating temperatures. A schematic of the doping dependence of carrier recombination mechanisms for both n-type and p-type LWIR HgCdTe ($\lambda_c = 10$ μm) at 77 K is shown in Fig. 5. The trend lines of carrier lifetimes for Auger recombination (Auger 1 and Auger 7) are given according to Kinch *et al.* [15].

Table 1.
Some physical properties of narrow gap semiconductors.

Material	E_g (eV)		μ_e (10^4 cm^2/Vs)		μ_h (10^4 cm^2/Vs)		n_i (cm^{-3})		ε
	77 K	300 K	77 K	300 K	77 K	300 K	77 K	300 K	
InAs	0.414	0.359	8	3	0.07	0.02	6.5×10^3	9.3×10^{14}	14.5
InSb	0.228	0.18	100	8	1	0.08	2.6×10^9	1.9×10^{16}	17.9
$In_{0.53}Ga_{0.47}As$	0.66	0.75	7	1.38		0.05		5.4×10^{11}	14.6
PbS	0.31	0.42	1.5	0.05	1.5	0.06	3×10^7	1.0×10^{15}	172
PbSe	0.17	0.28	3	0.10	3	0.10	6×10^{11}	2.0×10^{16}	227
PbTe	0.22	0.31	3	0.17	2	0.08	1.5×10^{10}	1.5×10^{16}	428
$Pb_{1-x}Sn_xTe$	0.1	0.1	3	0.12	2	0.08	3.0×10^{13}	2.0×10^{16}	400
$Hg_{1-x}Cd_xTe$	0.1	0.1	20	2	0.044	0.01	3.2×10^{13}	2.3×10^{16}	18.0
$Hg_{1-x}Cd_xTe$	0.25	0.25	8	1	0.044	0.01	7.2×10^8	2.3×10^{15}	16.7

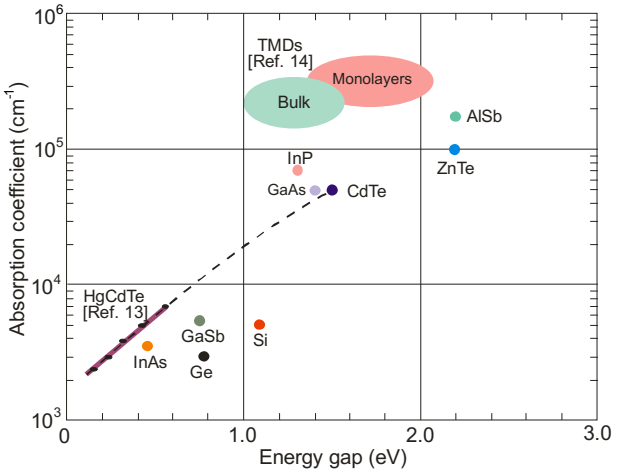

Fig. 4. Comparison of absorption coefficients and energy bandgaps at room temperature for a variety of semiconductor materials. The TMDs (both bulk and monolayers) of Mo and W are taken after Ref. 14.

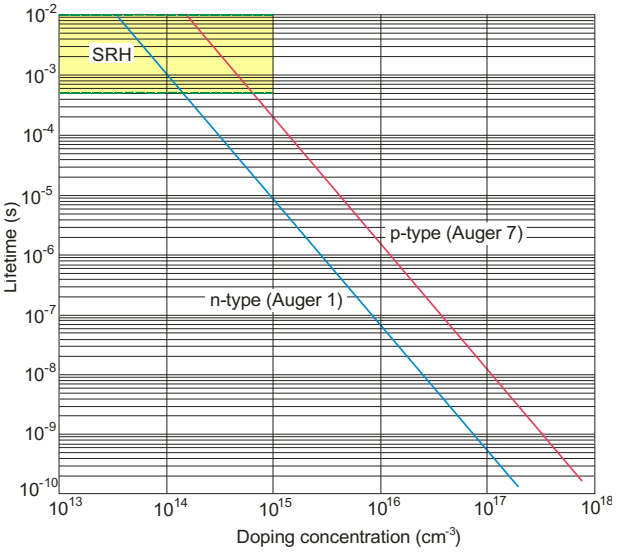

Fig. 5. Dependence of the carrier lifetimes as a function of doing concentration for LWIR HgCdTe at 77 K. Theoretical trend lines for n-type and p-type materials are taken after Ref. 15. A lower limit to the SRH lifetime of 10 ms has been demonstrated in lightly doped active regions for the MWIR detectors and 0.5 ms for the LWIR detectors.

The Shockley-Read-Hall (SRH) mechanism is responsible for lifetimes in lightly doped n- and p-type HgCdTe. Residual impurities and native defects create the SRH centres. However, this mechanism is currently unknown. According to a recently published paper [16], it has been shown that the lower limit to the SRH lifetime is 10 ms for the MWIR detectors and 0.5 ms for the LWIR detectors. These values can be approximated for HOT conditions [4].

HgCdTe is one of the few materials that has sufficiently long recombination lifetimes what allows to suppress the dark current of an LWIR photodiode operating at 300 K to be limited by the background radiation from the surrounding environment.

3.2. 2D materials—general outlook

The gapless nature of graphene affects the high dark current which significantly reduces sensitivity and limits further development of graphene-based infrared photodetectors. Hybrid graphene-based detectors are characterized by a limited linear dynamic range due to a charge relaxation time which leads to a decrease in sensitivity with increasing optical power. For these reasons, a new development path for IR photodetectors is towards alternative 2D materials.

2D materials are layered van der Waals (vdW) solids. The atomic layers are formed in such a way that the in-plane atoms are connected by ionic or tight covalent bonds along the 2D directions. Each atomic layer is connected to each other by weak vdW interactions along the out-of-plane direction. This anisotropy of properties affects the fact that many 2D materials can be mechanically exfoliated from bulk crystalline materials. Moreover, due to the weak physical bonds between individual layers, it is possible to combine different 2D materials together with the possibility of free formation of heterostructures.

The band structures of layered materials differ from their bulk counterparts. For example, in the case of transition metal dichalcogenides (TMDs), the band structure transits from a smaller indirect transition to a larger direct one due to quantum confinement effects [17]. Thus, the bandgap can be tuned by changing the number of layers and TMDs can detect light at different wavelengths. Furthermore, the large strains that occur in these materials strongly affect their optical and electronic properties.

TMDs show much higher absorption per unit thickness as compared to Si and GaAs (see Fig. 4). This figure shows the inherent trade-off between bandgap and absorption. The high absorption coefficient of TMDs (typically of the order of more than 10^5 cm^{-1}) is due to the dipole transitions between the localized d-states and the excitonic coupling of such transitions. They have some of the highest absorption coefficients among known materials. However, these high absorption coefficients are limited to wide band gaps between 1 and 2 eV. Figure 6 shows the spectral absorption coefficient for selected materials, including Si and GaAs. The absorption coefficient of GaAs for a light energy of 2 eV is smaller by one order of magnitude compared to MoS_2. In the longer wavelength range, typical of the infrared spectrum, absorption coefficients are much lower (see Fig. 3).

The carrier mobility of TMD films (like $PtSe_2$, PtS_2, and $PdSe_2$) and black phosphorus (bP) on back-gated SiO_2 substrates is low (typically less than 250 cm^2/Vs [18])

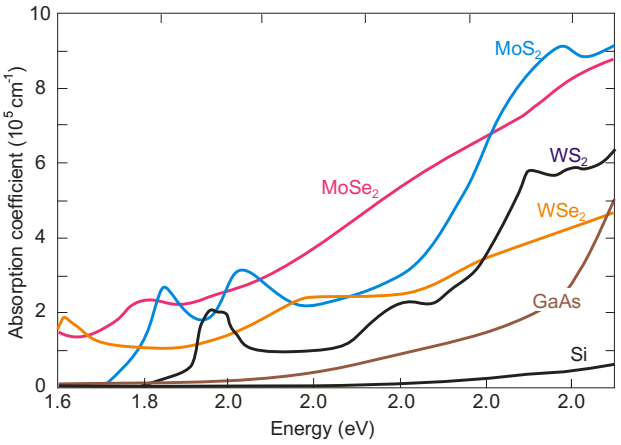

Fig. 6. Spectral dependence of the absorption coefficients for selected semiconductors (after Ref. 14).

compared to the electron mobility in LWIR HgCdTe (typically about 10^4 cm^2/Vs). Although the mobility can be increased by increasing the number of TMDs layers, the low mobility values are difficult to overcome. The main factors limiting carrier mobility are ripples, phonon scattering, impurity scattering, and interface scattering.

Therefore, the design of light traps and special device architectures (including hybrid structure with photogating effect, plasmonic metal particles, shells, or resonators) plays a key role in enabling the design of efficient 2D semiconductor photodetectors in the ultra-low thickness limit.

4. Detector materials figure of merit

As is shown in (1), the detector detectivity depends on the α/G_{th} ratio. The thermal generation rate, G_{th}, is defined as the rate at which a perturbed carrier system returns to equilibrium. For example, in a reversed-biased photodiode, it represents the rate at which carriers are generated within the diffusion length of the junction. As is shown by Kinch [4], the carrier generation rate can be expressed by:

$$G_{th} = \frac{N_{min} t}{\tau}, \tag{10}$$

where N_{min} is the minority carrier density, t is the detector thickness, and τ is the carrier lifetime. Since a typical detector thickness is $t = 1/\alpha$, where α is the absorption coefficient, then:

$$G_{th} = \frac{N_{min}}{\alpha\tau}. \tag{11}$$

The thermal generation rate of minority carriers (e.g., holes in n-type absorption region of the HgCdTe photodiode) is equal to:

$$G_{th} = \frac{N_{min}}{\alpha\tau} = \frac{n_i^2}{N_{maj}\alpha\tau}, \tag{12}$$

where N_{maj} is the majority carrier density and n_i is the intrinsic carrier concentration. In this case, the photodiode detectivity depends on:

$$D^* \propto \left(\frac{\alpha}{G_{th}}\right)^{1/2} = \left(\frac{\alpha^2 N_{maj}\tau}{n_i^2}\right)^{1/2} = \left(\frac{\sqrt{N_{maj}}}{n_i}\right)\alpha\sqrt{\tau}, \tag{13}$$

i.e., the detectivity is proportional to the product of $\alpha\sqrt{\tau}$.

It follows from the last formula that the material of the detector active region should have the highest possible values for the absorption coefficient and the carrier lifetime.

As is shown in Fig. 5, the demonstrated carrier lifetime in the HgCdTe ternary alloy is at the millisecond level and is about six orders of magnitude higher than for 2D materials such as TMDs (MoS_2, $MoSe_2$, and WSe_2) (see Fig. 7).

Considering the experimental data collected in Figs. 4, 5, and 7, it is possible to compare the estimated $\alpha\sqrt{\tau}$ values for HgCdTe ($\alpha = 2\times10^3$ cm^{-1}, $\tau = 10^{-3}$ s) with those for 2D TMD materials ($\alpha = 2\times10^5$ cm^{-1}, $\tau = 10^{-9}$ s). For HgCdTe, it is equal to $2\times10^2/\sqrt{10}$ s$^{1/2}$/cm while for TMD materials: $2\times10^1/\sqrt{10}$ s$^{1/2}$/cm. Note that the comparison of $\alpha\sqrt{\tau}$ values is for semiconductors with significantly different energy gaps. For a hypothetical 2D material with a narrow energy gap (of the order of 0.1 eV which is the case of HgCdTe), the absorption coefficient would be smaller (about one order of magnitude), resulting in a much smaller $\alpha\sqrt{\tau}$ for the hypothetical 2D materials compared to the HgCdTe material.

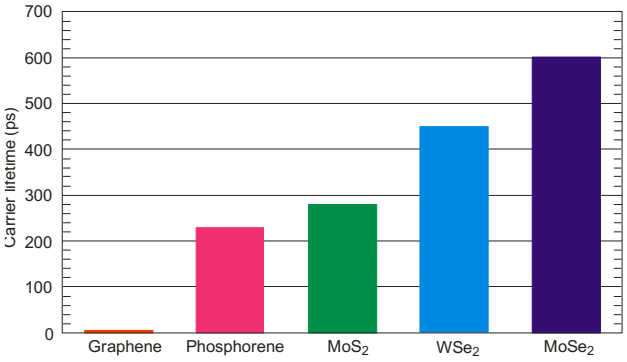

Fig. 7. Carrier lifetimes in different 2D materials (after Ref. 19).

To summarize the discussion in this section, it can be concluded that, considering the $\alpha\sqrt{\tau}$ paradigm, HgCdTe is a better material for the active area of LWIR detectors compared to 2D TMD materials.

5. High operating temperature LWIR photodetectors

Hitherto, two material systems have been used in the fabrication of LWIR FPAs: HgCdTe ternary alloy and III-V structures based on type-II superlattices (T2SLs). The position of the second class of materials has increased due to implementation of novel structures like barrier detectors, e.g., nBn structures. Recently, Rogalski *et al.* have critically analysed the performance of both classes of photodetectors [20]. The following is clear from their work:

- *"III-V materials have inherently short Shockley-Read lifetimes below 1 μs, and require nBn architecture to operate at reasonable temperatures, and as such are diffusion current limited. This applies both to the simple alloy and the T2SL versions,*
- *HgCdTe alloys have long Shockley-Read lifetimes > 100 μs depending on the cut-off wavelength. They can thus operate with either architecture, and may be diffusion or depletion current limited,*
- *III-Vs offer similar performance to HgCdTe at an equivalent cut-off wavelength, but with a sizeable penalty in operating temperature, due to the inherent difference in Shockley-Read lifetimes.*

Important advantage of T2SLs is the high quality, high uniformity and stable nature of the material. In general, III-V semiconductors are more robust than their II-VI counterparts due to stronger, less ionic chemical bonding. As a result, III-V-based FPAs excel in operability, spatial uniformity, temporal stability, scalability, producibility, and affordability – the so-called "ibility" advantages" [21]. Moreover, the status of III-Vs materials can be strengthened since Hg-containing devices can potentially lead to health and environmental concerns, so evaluation of alternative materials is required.

In the well-known Kinch's monograph [4], it is proved that "*the ultimate cost reduction for an IR system will only be achieved by the room temperature operation of arrays with pixel densities that are fully consistent with background and diffraction-limited performance due to the system optics*". After sixty years of history of HgCdTe (its discovery was announced in 1959 [22]), this material system meets the above requirements and is still in a privileged position. To achieve this goal, a doping concentration in active i-region of a P-i-N heterojunction photodiode below 5×10^{13} cm^{-3} is required. This level of doping and experimental data supporting theoretical predictions for fully depleted HgCdTe FPAs has been demonstrated by Teledyne Technologies [16, 23]. Under these circumstances, the evaluation for assessing the merit of HgCdTe detectors relative to novel III-V devices with respect to performance and costs may change.

Trends in the performance limitations of HOT IR photodetectors have been considered in a recent paper [6] taking into account different material systems: HgCdTe, T2SLs, 2D materials, and colloidal quantum dots. Here, more attention is directed towards 2D materials and HgCdTe.

As evidenced by several recently published papers [4, 16, 23, 24], at the current stage of the HgCdTe technology development, the Rule 07 metric (specified in 2007 [25]) is not an appropriate approach to predict the HgCdTe detector system performance and as a reference benchmark for alternative technologies. In 2019, Lee *et al.* [23] proposed replacing Rule 07 with "Law 19" and presented a comparison of this fundamental limit with Rule 07.

Figure 8 collects the highest detectivity values published in the literature for IR photodetectors operating at room temperature in the MWIR and LWIR region, including single-element ones for 2D material [26–31]. This fact should be clearly emphasised, since the detectivity data marked for commercial photodetectors are typical for pixels in IR FPAs. Commercially available HgCdTe photodetectors are sub-BLIP devices [32, 33]. Figure 8 also shows the theoretical prediction of the ultimate performance calculated for P-i-N HOT HgCdTe photodiodes assuming a value of τ_{SRH} = 1 ms, an absorber doping level of 5×10^{13} cm^{-3}, and an active region thickness of t = 5 μm. Details of the calculations are described in Ref. 6. As shown, the detectivity of low-doping P-i-N HgCdTe (5×10^{13} cm^{-3}) photodiodes, operating at room temperature in a spectral band above 3 μm, is limited by background radiation (at D^* level above 10^{10} Jones, it is not limited by detector itself) and can be improved more than an order of magnitude over that predicted by Rule 07.

6. Record detectivities of LWIR 2D material photodetectors

As shown in Fig. 8, the performance of several single element 2D material photodetectors operating at room temperature in the MWIR and LWIR regions is comparable to or higher than standard commercial HgCdTe photodetectors. Table 2 shows additional parameters characterising state-of-the-art 2D material photodetectors [31, 34–38]. Black phosphorus instability of the surface due to a chemical degradation in ambient conditions (highly hygroscopic, tending to take up moisture from the air) remains the major impediment to its prospective applications. More promising are stable TMD photodetectors such as the $PdSe_2/MoS_2$, and WS_2/HfS_2 heterojunctions with a record detectivity in the LWIR range at room temperature [31]. The WS_2/HfS_2 detector operation is based on the absorption of interlayer excitons. This heterostructure photoconductor (like phototransistor) has been operated with a voltage between drain and source to dissociate the interlayer excitons and extracts free carriers.

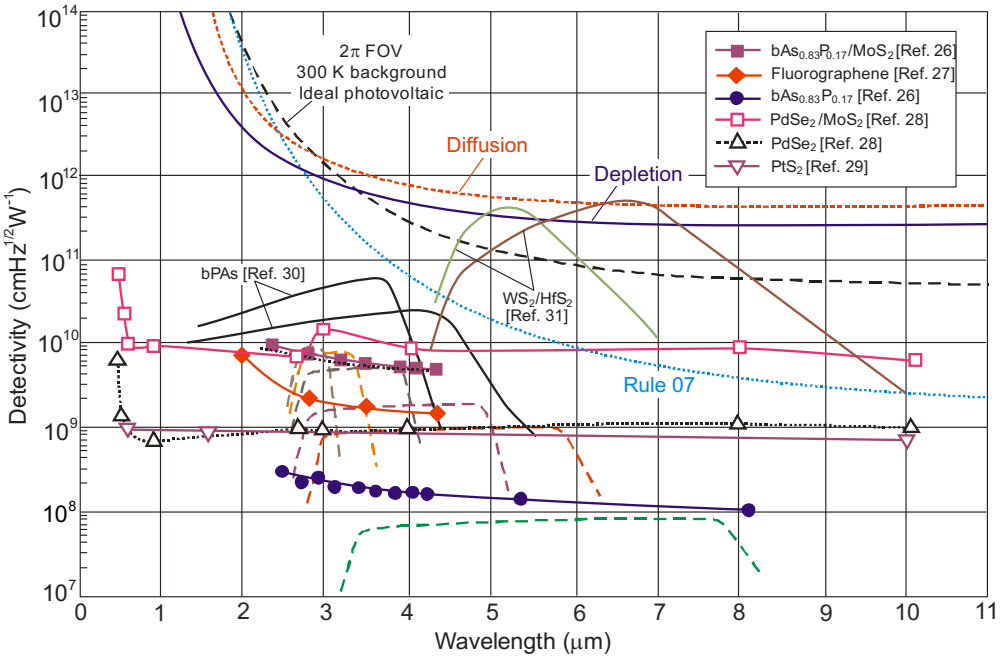

Fig. 8. Spectral dependence of detectivity for the currently employed room-temperature operating HOT HgCdTe photodiodes (dashed lines, Ref. 32) and different types of 2D material photodetectors. The additional data are taken from literature as marked. The theoretical curves are calculated for P-i-N HOT HgCdTe photodiodes assuming the value of τ_{SRH} = 1 ms, the absorber doping level of 5×10^{13} cm^{-3}, and the thickness of active region t = 5 μm. Details of theoretical calculations are described in Ref. 6.

Table 2.
The state-of-the-art 2D materials MW and LW infrared photodetectors.

Photodetector	Response time	Optimal wavelength (μm)	Responsivity (A/W)	Detectivity ($cmHz^{1/2}/W$)	References
bP	-	3.68	23	-	[35]
bP/MoS_2	4 μs	3.60	0.9	1.1×10^{10}	[36]
WS_2/HfS_2	2.2 ms	5.2 6.7	$\sim2\times10^3$ $\sim3\times10^3$	$\sim4\times10^{11}$ $\sim7\times10^{11}$	[31]
$PtSe_2$	1.1 ms	10	4.5	7×10^8	[37]
TiO_2/Gr	2.6 ms	10	300	7×10^8	[38]

The gate voltage has been changed in a wide range between +40 V to −40 V. The high responsivity values for these heterostructures (above 10^3 A/W, see Table 2) indicate a large photogating effect.

The authors of Ref. 31 have evaluated the record detectivity of WS_2/HfS_2 heterojunction to be of about 5×10^{11} $cmHz^{1/2}/W$ at room temperature in the spectral region of 5 to 8 μm—this detectivity value is higher than the BLIP limited value for a 2π field of view and a 300 K background. This fact of a great historical significance was not noticed by the authors. Detectivity is overestimated. It is not clear how it was estimated.

In the estimation of the detectivity of 2D material photodetectors, influence of different types of noise should be taken into account:

- usually, the shot noise is considered as the main source of noise in layered detectors,
- however, for photodetectors operating at room temperature with high photogain and low-response speed induced by the long carrier lifetime (which is the case in Ref. 31), both thermal noise and generation-recombination (g-r) noise cannot be neglected; the contribution of light-induced g-r noise is significant,
- also, the low-frequency noise (1/*f*) should be investigated as an important metric for evaluating the detector performance.

For the above reasons, it is rather problematic to approve such high detectivity, close to 10^{12} $cmHz^{1/2}/W$ at 6.5 μm, as a practical value at room temperature.

The design of WS_2/HfS_2 heterojunctions (phototransistors) compared to P-i-N depleted HgCdTe photodiodes affects additional disadvantage in the future array fabrication—phototransistors require three contact devices (compared to two photodiode contacts) which results in a higher power consumption of the arrays and limits their fill factor.

The evaluations presented above consider the general issues related to achieving the BLIP performance of LWIR photodetectors operating under HOT conditions and may change the calculus of the advantages of 2D material photodetectors over HgCdTe photodiodes in terms of performance.

7. High operating temperature LWIR arrays: HgCdTe *vs.* 2D materials

During the development of LWIR focal plane arrays, more attention has been focused on photovoltaic devices. Compared to photoconductors, photodiodes are characterized by very low power dissipation, inherently high impedance, negligible 1/*f* noise, and easy multiplexing on a silicon focal plane chip. Under these conditions, they are assembled in 2D arrays containing a very large number of elements (up to 10^8 pixels), limited only by the current stage of technology development. When operating in reverse bias, their impedances increase, facilitating electrical matching to compact low-noise silicon readout preamplifier circuits. In addition, a rapid photocarrier accumulation by the junction affects the linear characteristics at much higher photon flux levels than for photoconductors.

Currently, single/point photodetectors are typically used to demonstrate 2D imaging sensors. The first 2D material sensors operating in the visible and short-wave infrared range have also been demonstrated [39]. A dual band vertical GaSe/GaSb heterostructure linear array (16×1) was fabricated using the MBE growth technique in 2017 [40]. Also, a 388×288 20-μm pixel graphene-colloidal quantum dot (Gr/QD hybrid photodetector) CMOS-based integrated sensor operated in the UV-visible-SWIR range from 300 to 2000 nm was demonstrated later [41]. The last array design has disadvantages:

- large pixel size limits spatial resolution compared to current commercial CMOS sensors operating in the visible region (smallest pixel sizes are of about 1 μm),
- poor operability of 95%,
- use of Gr/QD hybrid pixels; despite their high photogain (of about 10^7) and responsivity (of above 10^7 A/W), these photodetectors are characterized by slow response time (>1 ms) [42] and, consequently, also limited linear dynamic range of operation,
- hybrid detector requires a three-contact device (like phototransistor) which affects the higher power consumption of the arrays and limits their fill factor,
- complex design of hybrid pixels (e.g., phototransitor *vs.* photodiode) also affects uniformity and operability of the array. It is well known that QD nonuniformity significantly limits the performance of QD photodetector arrays [43].

As noted in section 5, III-Vs materials offer similar performance to HgCdTe at an equivalent cut off wavelength but require a lower operating temperature. However, an important advantage of III-Vs materials is their high quality, high uniformity, and material stability. The HRL Laboratories research group has demonstrated high definition-format (1280×720, 12-μm pitch) T2SL

dual-band MWIR/LWIR FPAs grown on GaSb substrates [21]. No degradation in either sensitivity or operability was observed after a reliability test performed by cycling the array temperature from 70 K to 290 K more than 2000 times.

At the current stage of the LWIR array technology development, the global market is dominated by HgCdTe FPAs. Table 3 collects representative parameters of commercial HgCdTe FPAs operating in the LWIR spectra region. The typical *NEDT* value is slightly above 20 mK with *f*/2 optics, integration time of $\tau_{int} \approx 0.2{-}0.3$ ms, and charge-handling capacity $N_w \approx 10^7$ electrons. LWIR arrays typically operate in the temperature range between 80 and 100 K. The commercial market share of 2TSL arrays is steadily increasing. However, it is now clear that 2TSL photodetectors are not competitive with HgCdTe photodiodes operating at near room temperature in the LWIR spectral range. The performance of so-called T2SL interband quantum cascade photodetectors (IB QCPs) is comparable with HgCdTe photodiodes, but their fabrication is challenging (complicated structure with many interfaces and strained thin layers), resulting in high fabrication costs [20].

At the current stage of the commercial technology development, LWIR HgCdTe photodiode arrays are typically operated at temperatures below 100 K to reduce detector noise due to various carrier transport mechanisms associated with the narrow band gap. Cooled technologies are expensive and for many applications unattractive due to their prohibitive size, weight, and power consumption. Nowadays, significant efforts are being made to reduce size, weight, and power consumption (SWaP) and, consequently, reduce the cost of imaging systems to increase operating temperature of HOT detectors. The ultimate goal is to produce a detector where the dark current is less than the system background flux current and in which the 1/*f* noise is negligible with respect to the background flux shot noise. Smaller pixels increase functionality of the imaging systems [5].

As is mentioned in section 5, Teledyne has recently developed technology of lightly doped P-i-N HgCdTe photodiode FPAs operating at a reverse bias compatible with CMOS readout [16, 23]. At reverse bias voltage typically of about 1–2 volts, free electrons in active i-region are removed and the dark current limited by Auger 1 recombination mechanism is suppressed to a level dominated by the background seen by detector. Thus, the background-dominated current is by a factor of 10 to 100 lower than predicted by Rule 07, depending on cut off wavelength and operating temperature.

The most critical array performance is required for Earth science, planetary science, and astronomy. Recently demonstrated fully depleted 640×512 arrays (in MWIR and LWIR operating up to 250 K and 160 K, respectively [16, 44]) have provided a unique capability to produce the largest format arrays. The Euclid array consisting of 16 H2RG devices (each with 2k×2k 18-μm pixel size) will be the largest IR array operating in space (67 million pixels) to be launched in 2022. Further technological refinement of P-i-N HgCdTe depleted photodiodes with lower doping levels in the active region (about 10^{13} cm^{-3} [6, 16]) is expected to increase the operating temperature of both MWIR and LWIR photodiodes to 300 K (see Fig. 9). It is expected that HgCdTe photodiode arrays for room-temperature operation in the MWIR range will be produced soon (in a few years), while the LWIR arrays will be produced in the longer term.

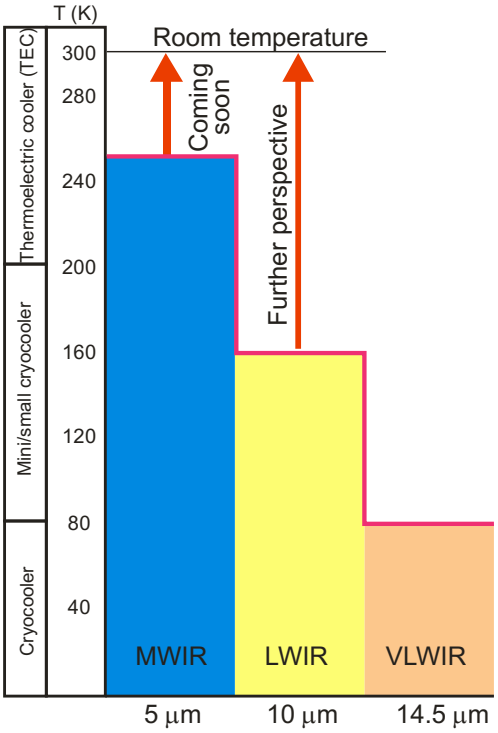

Fig. 9. Increase in operating temperature of HgCdTe FPAs.

Table 3.
Representative HgCdTe LWIR hybrid FPAs.

Manufacturer/Website	Size/Architecture	Pixel size (μm)	Spectral range (μm)	Oper. temp. (K)	*NETD* (mK) (*F* number, τ_{int})	Operability (%)
Lynred (France) www.lynred.com/products	640×512 (Scorpio)	15×15	7.7–9.3	80	22	>99.8
Leonardo (Great Britain) www.leonardocompany.com	640×512 (Hawk LW)	16×16	8–10	up to 90	23 (0.2 ms)	>99.8
	1024×768 (Merlin LW)	16×16	8–10	up to 90	23	>99
	640×512 (CondorII)	24×24	MW/LW (dual)	80	28/28	>99
IAM (Germany) www.aim-ir.com	640×512	15×15	7.6–9.0	70	23 (*f*/2, 0.4 ms)	>99.3
	1280×1024	15×15	7.6–9.0	70	30 (*f*/2, 0.3 ms)	>99

Although 2D materials platform has announced the introduction of many HOT LWIR single photodetectors, there are still challenges to implement the real potential and exploit the distinct advantages of new 2D crystals. Large-scale production of high-quality 2D materials at low cost and establishing large-scale integration of 2D crystals into existing photonic and electronic (CMOS-based) platforms are required to achieve the successful commercialisation. However, their record-breaking results published in the literature are unreliable as their values exceed the physical limit set by the influence of background radiation in the LWIR range for detectors operating at room temperature.

Current 2D materials research is mostly limited to materials exfoliated from bulk layered crystals, with very limited yields, reproducibility, and scalability. Consequently, the divergence in responsivity and response time values is large [45–47], of about 8 orders of magnitude mainly in visible and near IR regions (see Fig. 10). Furthermore, Figure 10(a) shows that some literature data [31, 48] are located above BLIP performance for a 2π FOV and 300 K in the background. These data are over-estimated.

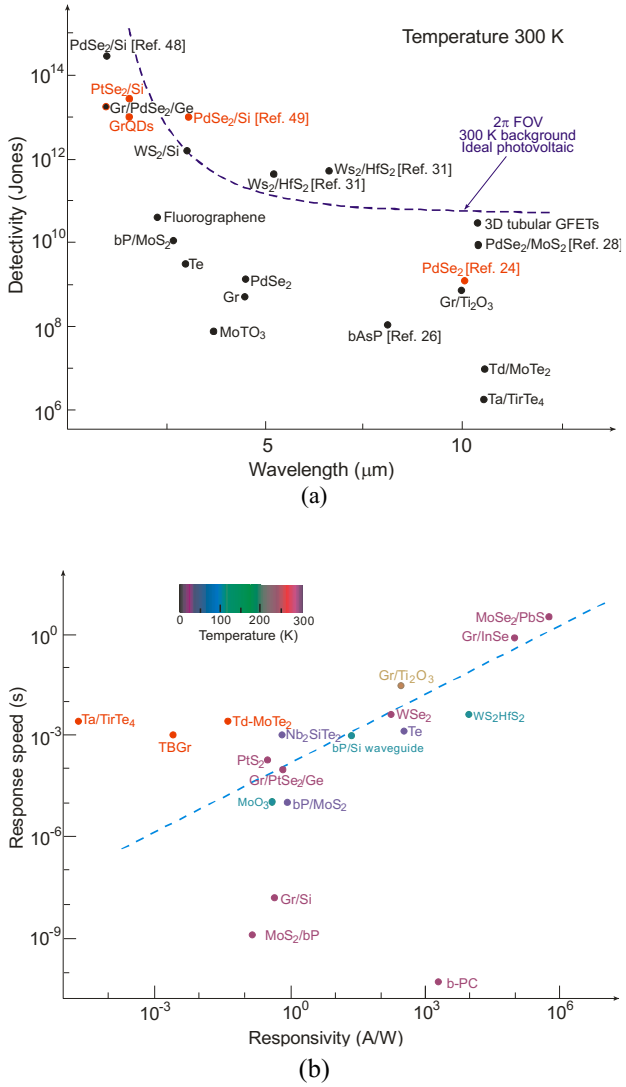

Fig. 10. Comparison of 2D material photodetector parameters: spectral detectivity at room temperature (a), current responsivity and speed response at different working temperature (adapted after Ref. 47) (b). Additional data are taken from literature as marked.

FPA manufacturing requires a homogeneous and large-scale production. At the current stage of technology development, 2D films have a small area (typically 100 μm^2) which makes them expensive for industrial applications. In addition, this technology is not mature which has a negative impact on the uniformity of pixel arrays. The development of efficient 2D photodetector arrays integrated in the focal plane of the imaging system is particularly important for industrial applications. Most experimental methods for transferring 2D materials from their substrates to the desired electronic circuits are either incompatible with high-volume production or lead to a significant degradation of the 2D material and its electronic properties.

However, the above difficulties in scaling wafer sizes from 2D materials may be overcome in the future. This is already noticeable, in particular, in the adaptation of 2D materials for a 2D transistor fabrication. For example, IMEC is introducing tungsten disulfide (WS_2) into the scaling roadmap for logic devices [50]. Recently, the European Commission launched a €20 million project to bridge the gap between lab-scale and high-volume production of electronic devices based on 2D materials [51].

8. Conclusions

Like graphene-based detectors, alternative 2D IR photodetectors are limited by the trade-off between high responsivity, ultrafast response time, and broadband operation. In general, due to their ultrathin structure, insufficient absorption leads to low quantum efficiency and detectivity. So far, the most promising performance of infrared detectors has been demonstrated for 2D TMD materials. Despite the strong light-matter interaction and high absorption coefficient, TMD materials are characterized by short carrier lifetimes and lower carrier mobilities than the HgCdTe alloy system. Despite these drawbacks, the record detectivity values for single photodetectors have been estimated for 2D material photodetectors in the LWIR range at room temperature. However, these are overestimated. Their performance is often estimated theoretically by assuming the dominant influence of shot noise (which is not always correct). Further research is needed to clarify the factors contributing to such high detectivities and confirm these exceptional results in practice, in a large-scale fabrication.

Current 2D materials research is mostly limited to materials exfoliated from bulk layered crystals with very limited yields, reproducibility, and scalability. FPA fabrication requires a homogeneous large-scale production. Conventional methods, such as CVD or transfer methods, lead to small sample sizes on the micrometers scale.

From the point of view of economic profitability and competitiveness in the future global market, the industrial production of detector arrays with high operability, spatial uniformity, temporal stability, scalability, producibility, and affordability is important. All these aspects are in the early stages of the 2D materials development and fabrication capabilities.

2D technology is unlikely to replace HgCdTe photodiodes in LWIR HOT devices within the next decade. The mature technology and the potential properties of HOT LWIR HgCdTe photodiodes operating in the range above

3 μm guarantee achieving the background-limited detectivity. However, it cannot be ruled out that after several decades of research, development and, most importantly, billions of dollars in investment at the national and international levels, the position of 2D materials will consolidate in the IR detector technology. These trends in the development of 2D materials for electronic devices (especially transistors) are already noticeable. 2D technology can coexist with, e.g., Si technology [52] due to fundamental limitations of Si at the nanometric scale [53]. It is expected that silicon second life will come from compatibility with other materials that will extend its capabilities.

Acknowledgements

This work was supported by the funds granted to the Faculty of Advanced Technologies and Chemistry, Military University of Technology, within the subsidy for maintaining research potential in 2021, grant no. UGB-842/2021.

References

[1] Rogalski, A. *2D Materials for Infrared and Terahertz Detectors.* (CRC Press, Boca Raton, 2020).

[2] Rogalski, A. *Infrared and Terahertz Detectors*. (CRC Press, Boca Raton, 2019).

[3] Rogalski, A. Quantum well photoconductors in infrared detector technology. *J. Appl. Phys.* **93**, 4355–4391 (2003). https://doi.org/10.1063/1.1558224

[4] Kinch, M. A. *State-of-the-Art Infrared Detector Technology*. (SPIE Press, Bellingham, 2014).

[5] Rogalski, A., Martyniuk P. & Kopytko, M. Challenges of small-pixel infrared detectors: a review. *Rep. Prog. Phys*. **79**, 046501-1–42 (2016). https://doi.org/10.1088/0034-4885/79/4/046501

[6] Rogalski, A., Martyniuk, P., Kopytko, M. & Hu, W. Trends in performance limits of the HOT infrared photodetectors. *Appl. Sci.* **11**, 501 (2021). https://doi.org/10.3390/app11020501

[7] Piotrowski J. & Rogalski, A. Comment on "Temperature limits on infrared detectivities of InAs/$In_xGa_{1-x}Sb$ superlattices and bulk $Hg_{1-x}Cd_xTe$" [J. Appl. Phys. **74**, 4774 (1993)]. *J. Appl. Phys*. **80**, 2542–2544 (1996). https://doi.org/10.1063/1.363043

[8] Robinson, J., Kinch, M., Marquis, M., Littlejohn, D. & Jeppson, K. Case for small pixels: system perspective and FPA challenge. *Proc. SPIE* **9100**, 91000I-1–10 (2014). https://doi.org/10.1117/12.2054452

[9] Holst G. C. & Lomheim, T. C. *CMOS/CCD Sensors and Camera Systems*. (JCD Publishing and SPIE Press, Winter Park, 2007).

[10] Holst, G. C. & Driggers, R. G. Small detectors in infrared system design. *Opt. Eng*. **51**, 096401-1–10 (2012).

[11] Boreman, G. D. *Modulation Transfer Function in Optical and Electro-Optical Systems*. (2nd edition) (SPIE Press, Bellingham, 2021).

[12] Higgins, W. M., Seiler, G. N., Roy, R. G. & Lancaster, R. A. Standard relationships in the properties of $Hg_{1-x}Cd_xTe$. *J. Vac. Sci. Technol*. A **7**, 271–275 (1989). https://doi.org/10.1116/1.576110

[13] Chu, J. H., Li, B., Liu, K. & Tang, D. Empirical rule of intrinsic absorption spectroscopy in $Hg_{1-x}Cd_xTe$. *J. Appl. Phys*. **75**, 1234 (1994). https://doi.org/10.1063/1.356464

[14] Jariwala, D., Davoyan, A. R., Wong, J. & Atwater, H. A. Van der Waals materials for atomically-thin photovoltaics: promise and outlook. *ACS Photonics* **4**, 2962−2970 (2017). https://doi.org/10.1021/acsphotonics.7b01103

[15] Kinch, M. A. *et al.* Minority carrier lifetime in p-HgCdTe. *J. Electron. Mater.* **34**, 880–884 (2005). https://doi.org/10.1007/s11664-005-0036-2

[16] Lee, D. *et al*. Law 19: the ultimate photodiode performance metric. *Proc. SPIE* **11407**, 114070X (2020). https://doi.org/10.1117/12.2564902

[17] Yang, Z., Dou, J. & Wang, M. Graphene, Transition Metal Dichalcogenides, and Perovskite Photodetectors. in *Two-Dimensional Materials for Photodetector* (ed. Nayak, P. K.) 1–20 (IntechOpen, 2018). http://doi.org/10.5772/intechopen.74021

[18] Pi, L., Li, L., Liu, K., Zhang, Q. Li, H. & Zhai, T. Recent progress on 2D noble-transition-metal dichalcogenides. *Adv. Funct. Mater*. **29**, 1904932 (2019). https://doi.org/10.1002/adfm.201904932

[19] Vargas-Bernal, R. Graphene Against Other Two-Dimensional Materials: A Comparative Study on the Basis of Photonic Applications. in *Graphene Materials* (eds. Kyzas, G. Z. & Mitropoulos, A. Ch.) 103–121 (IntechOpen, 2017). http://doi.org/10.5772/67807

[20] Rogalski, A., Martyniuk, P. & Kopytko, M. Type-II superlattice photodetectors versus HgCdTe photodiodes. *Prog. Quantum Electron.* **68**, 100228 (2019). https://doi.org/10.1016/j.pquantelec.2019.100228

[21] Delaunay, P. Y., Nosho, B. Z., Gurga, A. R., Terterian, S. & Rajavel, R. D. Advances in III-V based dual-band MWIR/LWIR FPAs at HRL. *Proc. SPIE* **10177**, 101770T-1–12 (2017). https://doi.org/10.1117/12.2266278

[22] Lawson, W. D., Nielson, S., Putley, E. H. & Young, A. S. Preparation and properties of HgTe and mixed crystals of HgTe-CdTe. *J. Phys. Chem. Solids* **9**, 325–329 (1959). https://doi.org/10.1016/0022-3697(59)90110-6

[23] Lee, D. *et al*. Law 19 – The Ultimate Photodiode Performance Metric. in *Extended Abstracts. The 2019 U.S. Workshop on the Physics and Chemistry of II-VI Materials* 13–15 (2019).

[24] Rogalski, A., Kopytko, M., Martyniuk, P. & Hu, W. Comparison of performance limits of HOT HgCdTe photodiodes with 2D material infrared photodetectors. *Opto-Electron. Rev.* **28**, 82–92 (2020). https://doi.org/10.24425/opelre.2020.132504

[25] Tennant, W. E., Lee, D., Zandian, M., Piquette, E. & Carmody, M. MBE HgCdTe technology: A very general solution to IR detection, described by 'Rule 07', a very convenient heuristic. *J. Electron. Mater.* **37**, 1406–1410 (2008). https://doi.org/10.1007/s11664-008-0426-3

[26] Long, M. *et al*. Room temperature high-detectivity mid-infrared photodetectors based on black arsenic phosphorus. *Sci. Adv.* **3**, e1700589 (2017). https://doi.org/10.1126/sciadv.1700589

[27] Du, S. *et al*. A broadband fluorographene photodetector. *Adv. Mater*. **29**, 1700463 (2017). https://doi.org/10.1002/adma.201700463

[28] Long, M. *et al*. Palladium diselenide long-wavelength infrared photodetector with high sensitivity and stability. *ACS Nano* **13**, 2511−2519 (2019). https://doi.org/10.1021/acsnano.8b09476

[29] Chen, Y. Unipolar barrier photodetectors based on van der Waals heterostructures. *Nat. Electron*. **4**, 357–363 (2021). https://doi.org/10.1038/s41928-021-00586-w

[30] Amani, M., Regan, E., Bullock, J., Ahn, G. H. & Javey, A. Mid-wave infrared photoconductors based on black phosphorus-arsenic alloys. *ACS Nano* **11**, 11724–11731 (2017). https://doi.org/10.1021/acsnano.7b07028

[31] Lukman, S. *et al*. High oscillator strength interlayer excitons in two-dimensional heterostructures for mid-infrared photodetection. *Nat. Nanotechnol*. **15**, 675–682 (2020). https://doi.org/10.1038/s41565-020-0717-2

[32] VIGO System Catalog 2018/2019. *VIGO System S.A.* https://vigo.com.pl/wp-content/uploads/2017/06/VIGO-Catalogue.pdf (2018).

[33] Mercury Cadmium Telluride Detectors. *Teledyne Judson Technologies LLC* http://www.teledynejudson.com/prods/Documents/MCT_shortform_Dec2002.pdf (2002).

[34] Zhong, F. *et al*. Recent progress and challenges on two-dimensional material photodetectors from the perspective of advanced characterization technologies. *Nano Res*. **14**, 1840–1862 (2021). https://doi.org/10.1007/s12274-020-3247-1

[35] Huang, L. *et al*. Waveguide integrated black phosphorus photodetector for mid-infrared applications. *ACS Nano* **13**, 913–921 (2019). https://doi.org/10.1021/acsnano.8b08758

[36] Bullock, J. *et al*. Polarization-resolved black phosphorus/molybdenum disulfide mid-wave infrared photodiodes with high detectivity at room temperature. *Nat. Photonics* **12**, 601–607 (2018). https://doi.org/10.1038/s41566-018-0239-8

[37] Yu, X. *et al*. Atomically thin noble metal dichalcogenide: a broadband mid-infrared semiconductor. *Nat. Commun.* **9**, 1545 (2018). https://doi.org/10.1038/s41467-018-03935-0

[38] Yu, X. *et al*. Narrow bandgap oxide nanoparticles coupled with graphene for high performance mid-infrared photodetection. *Nat. Commun.* **9**, 4299 (2018). https://doi.org/10.1038/s41467-018-06776-z

[39] Long, M., Wang, P., Fang, H. & Hu. W. Progress, challenges, and opportunities for 2D material-based photodetectors. *Adv. Funct. Mater.* 1803807 (2018). https://doi.org/10.1002/adfm.201803807

[40] Wang, P. *et al*. Arrayed van der Waals broadband detectors for dual-band detection. *Adv. Mater.* **29**, 1604439 (2017). https://doi.org/10.1002/adma.201604439

[41] Goossens, S. *et al*. Broadband image sensor array based on graphene–CMOS integration. *Nat. Photonics* **11**, 366–371 (2017). https://doi.org/10.1038/nphoton.2017.75

[42] Konstantatos, G. *et al*. Hybrid graphene-quantum dot phototransistors with ultrahigh gain. *Nat. Nanotechnol.* **7**, 363–368 (2012). https://doi.org/10.1038/nnano.2012.60

[43] Phillips, J. Evaluation of the fundamental properties of quantum dot infrared detectors. J. Appl. Phys. **91**, 4590–4594 (2002). https://doi.org/10.1063/1.1455130

[44] Jerram P. & Beletic, J. Teledyne's high performance infrared detectors for space missions. Proc. SPIE **11180**, 111803D-2 (2018). https://doi.org/10.1117/12.2536040

[45] Buscema, M. *et al*. Photocurrent generation with two-dimensional van der Waals semiconductor. Chem. Rev. **44**, 3691–3718 2015. https://doi.org/10.1039/C5CS00106D

[46] Wang, J. *et al*. Recent progress on localized field enhanced two-dimensional material photodetectors from ultraviolet-visible to infrared. *Small* **13**, 1700894 (2017). https://doi.org/10.1002/smll.201700894

[47] An, J. *et al*. Research development of 2D materials-based photodetectors towards mid-infrared regime. *Nano Select* **2**, 527 (2021). https://doi.org/10.1002/nano.202000237

[48] Wu, D. *et al*. Mixed-dimensional $PdSe_2$/SiNWA heterostructure based photovoltaic detectors for self-driven, broadband photodetection, infrared imaging and humidity sensing. *J. Mater. Chem. A* **8**, 3632–3642 (2020). https://doi.org/10.1039/C9TA13611H

[49] Zeng, L.-H. *et al*. Controlled synthesis of 2D palladium diselenide for sensitive photodetector applications. *Adv. Funct. Mater.* **29**, 1806878 (2019). https://doi.org/10.1002/adfm.201806878

[50] Imec shows excellent performance in ultra-scaled FETs with 2D-material channel. *Imec*. https://www.imec-int.com/en/articles/imec-shows-excellent-performance-in-ultra-scaled-fets-with-2d-material-channel (2019).

[51] Scaling Up Large-area Integration of 2D Materials. *Compound Semiconductor*. https://compoundsemiconductor.net/article/112712/Scaling_Up_Large-area_Integration_Of_2D_Materials (2021).

[52] Briggs, N. *et al*. A roadmap for electronic grade 2D materials. *2D Mater*. **6**, 022001 (2019). https://doi.org/10.1088/2053-1583/aaf836

[53] IRDS International Roadmap for Devices and Systems™ 2018 Update. *IEEE*. https://irds.ieee.org/images/files/pdf/2018/2018IRDS_MM.pdf (2018).

Update

Opto-Electronics Review 30 (2022) e141441

DOI: https://doi.org/10.24425/opelre.2022.141441

PAN POLISH ACADEMY OF SCIENCES

Opto-Electronics Review

journal homepage: https://journals.pan.pl/opelre

Corrigendum to "Van der Waals materials for HOT infrared detectors: A review" [Opto-Electronics Review 30 (2022) e140551]

Antoni Rogalski

Institute of Applied Physics, Military University of Technology, 2 Kaliskiego St., 00-908 Warsaw, Poland

Article info

Available on-line 11 May. 2022

Original article:
https://doi.org/10.24425/opelre.2022.140551

The author regrets that an error in equation (10) (detector thickness, *t*, should be removed) consequently affected the erroneous form of equation (13).

The correct version of the expression (10) is in the form of

$$G_{th} = \frac{N_{min}}{\tau},$$

which leads to expression (13) in the form of

$$D^* \propto \left(\frac{\alpha}{G_{th}}\right)^{1/2} = \left(\frac{\alpha N_{maj}\tau}{n_i^2}\right)^{1/2} = \left(\frac{\sqrt{N_{maj}}}{n_i}\right)\sqrt{\alpha\tau}$$

i.e. the detectivity is proportional to $\sqrt{\alpha\tau}$; not proportional to $\alpha\sqrt{\tau}$ as stated in the source paper.

As a result of the above correction, the last two paragraphs of section 4 have been amended as shown below:

Considering the experimental data collected in Figs. 4, 5 and 7, it is possible to compare the estimated $\sqrt{\alpha\tau}$ values for HgCdTe ($\alpha = 2\times10^3$ cm^{-1}, $\tau = 10^{-3}$ s) with those for 2D TMD materials ($\alpha = 2\times10^5$ cm^{-1}, $\tau = 10^{-9}$ s). For HgCdTe, it is equal to 1.4 (s/cm)$^{1/2}$ while for TMD materials: 1.4×10^{-2} (s/cm)$^{1/2}$, which is two orders of magnitude smaller. Note that the comparison of $\sqrt{\alpha\tau}$ values is for semiconductors with significantly different energy gaps. For a hypothetical 2D material with a narrow energy gap (of the order of 0.1 eV which is the case of HgCdTe), the absorption coefficient would be smaller (about one order of magnitude), resulting in a much smaller $\sqrt{\alpha\tau}$ for the hypothetical 2D materials compared to the HgCdTe material.

To summarize the discussion in this section, it can be concluded that, considering the $\sqrt{\alpha\tau}$ paradigm, HgCdTe is a better material for the active area of LWIR detectors compared to 2D TMD materials.

The corrections made changed the performance figure-of-merit values for the materials used in the fabrication of infrared detectors, but do not affect the qualitative conclusions cited throughout the paper.

*Corresponding author at: antoni.rogalski@wat.edu.pl

https://doi.org/10.24425/opelre.2022.141441
1896-3757/ Association of Polish Electrical Engineers (SEP) and Polish Academic of Sciences (PAS). Published by PAS